Journal Pre-proof

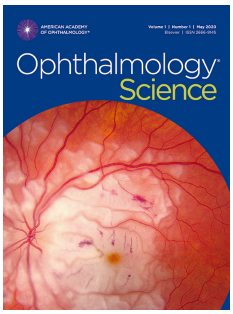

Optimizing retinal thermofusion in retinal detachment repair: achieving instant adhesion without air tamponade

Wilson J. Heriot, Andrew B. Metha, Zheng He, Jeremiah K.H. Lim, Anh Hoang, Tomoharu Nishimura, Mali Okada, Bang V. Bui

PII: S2666-9145(22)00068-9

DOI: https://doi.org/10.1016/j.xops.2022.100179

Reference: XOPS 100179

To appear in: *Ophthalmology Science*

Received Date: 27 January 2022

Revised Date: 25 May 2022

Accepted Date: 6 June 2022

Please cite this article as: Heriot W.J, Metha A.B, He Z., Lim J.K.H., Hoang A., Nishimura T., Okada M. & Bui B.V., Optimizing retinal thermofusion in retinal detachment repair: achieving instant adhesion without air tamponade, *Ophthalmology Science* (2022), doi: https://doi.org/10.1016/j.xops.2022.100179.

Optimizing retinal thermofusion in retinal detachment repair: achieving instant adhesion without air tamponade

Wilson J Heriot[1,2,3], Andrew B Metha[3], Zheng He[3], Jeremiah K.H. Lim[3,4], Anh Hoang[2,3], Tomoharu Nishimura[3,5], Mali Okada[2], Bang V. Bui[3]

1. Retinology Institute, Glen Iris, Victoria, Australia
2. Centre for Eye Research Australia, East Melbourne, Victoria, Australia
3. Department of Optometry and Vision Sciences, University of Melbourne, Parkville, Victoria, Australia
4. Caring Futures Institute, Flinders University, Bedford Park, South Australia, Australia
5. Department of Ophthalmology, Dokkyo Medical University Saitama Medical Center, 2-1-50 Minami-Koshigaya, Koshigaya, Saitama, 343-8555, Japan

Corresponding author:

A/Prof Wilson Heriot

Centre for Eye Research Australia, East Melbourne, Victoria, Australia

email: wheriot@unimelb.edu.au

Keywords: Pars plana vitrectomy, retinopexy, tamponade, rhegmatogenous retinal detachment repair, laser, dehydration, retinal thermofusion, retinal adhesion strength, tamponade independent

Abstract

Purpose

Rhegmatogenous retinal detachment repair by intraoperative sealing of the tear without a tamponade agent should enable faster restoration of vision, resumption of normal activities. It avoids the need for further surgery in the case of silicone oil endotamponade. This study evaluates the retinal thermofusion (RTF) retinopexy method of subretinal space dehydration prior to photocoagulation to create an instantaneous intraoperative retina reattachment in a preclinical model.

Design

Preclinical study.

Participants

20 Dutch Belt pigmented rabbits underwent RTF repair following experimental retinal detachment.

Method

In our *ex vivo* model, using post-mortem porcine or human retina (6 x 12mm) we quantify adhesion force between the retina and the underlying retinal pigment epithelium and choroid following treatment of one retinal edge. We compare (i) control, (ii) laser photocoagulation alone (iii) dehydration alone and (iv) dehydration followed by photocoagulation (RTF). Optimized parameters for RTF were then applied in the *in vivo* rabbit model of retinal detachment. Animals were followed for 14 days.

Main Outcome Measures

For our *ex vivo* model we measured adhesion force and related this to tissue temperature. For the *in vivo* study, we assessed retinal attachment using fundoscopy and histology.

Results

Using our *ex vivo* model we showed that RTF repair produced significantly higher adhesion force compared with photocoagulation alone independent of dehydration method: warm (60^{o}C) high air flow (50-70ml/min) or using laser wavelengths targeting water absorption peaks (1470 nm or 1940nm) with coaxial low air flow (10-20ml/min). The latter approach produced a smaller footprint of dehydration. Application of RTF (1940nm laser with coaxial air flow) in an *in vivo* retinal detachment model in rabbit eyes resulted in immediate retinal adhesion, achieving forces similar to the *ex vivo* experiments. RTF repair resulted in stable re-attachment of the retina over the two week follow up period.

Conclusions

We show that a short preliminary dehydrating laser treatment of a retinal tear margin prior to traditional laser photocoagulation creates an immediate intraoperative waterproof retinopexy adhesion independent of tamponade and of a wound-healing response. This approach will potentially allow rapid postoperative recovery irrespective of the tear location and improved vision.

Introduction

The essential outcome for successful rhegmatogenous retinal detachment (RRD) repair is closing the communication between the vitreous cavity and the subretinal space. Current retinopexy techniques do not create an instantaneous seal or strong retinal adhesion to the underlying retinal pigment epithelium (RPE) and choroid intraoperatively - as demonstrated clinically by retinal slippage during fluid-gas exchange for giant retinal tear repair[1]. The current method for retinal detachment repair is based on century-old principles established by Jules Gonin,[2-4] whereby a thermal tissue injury (heat or cold) triggers an inflammatory "wound healing" reaction that binds the retinal tear(s) margin to the underlying RPE and choroid.[5] Wound healing requires both time and continuous contact between the injured tissues to form a strong bond[6, 7] just as repair of a skin incision relies initially on sutures, tape or other support. Currently retinal and choroidal contact is achieved with an extraocular scleral buckle, or, more commonly, vitreoretinal surgery (vitrectomy) with a gas or liquid tamponade agent.[8, 9] When the tamponade is a gas, vision can be blocked for several weeks, most patients are unable to continue working, mobility is restricted and driving prohibited.[10] Critically, air travel or aeromedical evacuation is prohibited due to the risk of blinding intraocular gas expansion as ambient cabin pressure decreases during ascent and flight[11-14]. Liquid tamponade agents (silicone oil or a heavier than water mixture with perfluorocarbon liquid) require a second procedure for removal and can be associated with a variety of complications[15] including oil maculopathy and glaucoma. Furthermore, to achieve optimal buoyancy effect of the tamponade, patients often need to posture in a certain position for up to a week following the procedure, particularly for inferior pathology. This relies on patient compliance and can be difficult in those with mobility or cognitive issues. Finally, the presence of a gas tamponade at the completion of surgery can contribute to greater risk of retinal displacement and aniseikonia.[16]

That retinal reattachment following vitrectomy without tamponade is possible was reported by Martinez-Castillo et al.[17] but others have been unable to reliably reproduce these results. Retinal detachment repair without tamponade requires a new reproducible surgical method to seal retinal tears intraoperatively that is preferably intuitive for trained surgeons and compatible with current vitreoretinal surgical systems.

These requirements prompted a re-examination of the basic pathophysiology of retinal adhesion formation (retinopexy) and led to the development of the "retinal thermofusion"[18] method. This method is based on the basic principles that neither aspiration of, nor displacement by heavier than water agents (such as perfluorocarbon liquid), can evacuate all the subretinal fluid (SRF) because of the physical properties of water – namely the cohesion between water molecules and the adhesion of water molecules to a surface. Subretinal fluid is near-Newtonian with relatively weak inter-molecular bonds (cohesion) holding water molecules together[19] and these are much weaker than the

adhesive force between water and surfaces. In addition, the cell membranes of the RPE and the retina are lipid, and thus hydrophobic, and are immiscible with water. It is proposed that the persistence of a fine layer of SRF facilitates retinal translocation and slippage during giant retinal tear repair - despite the clinical appearance that the retina has been "reattached". Crucially, the fine layer of SRF maintains separation of the outer retina from the RPE such that photocoagulation coagulates both tissues sequentially and independently - the RPE and choroid is coagulated by heat generated by melanin absorption of laser energy and the retina is indirectly coagulated by the choroidal heat transferred via the SRF. The laser coagulation of the RPE and choroid separately to the retina prevents instantaneous integration of the two such that a wound healing process is required to create a permanent connection between the tissues.

Based on the preliminary method of retinal thermofusion where subretinal dehydration was achieved with a room temperature air stream[18], we have investigated a variety of methods to achieve subretinal space dehydration and measured the adhesion strength created by laser photocoagulation, both with and without subretinal space dehydration. We also developed a novel laser-based device comprising wavelengths that liberate water molecules from the water phase without significant elevation of tissue temperature to coagulation levels which, when combined with a low-flow coaxial airstream, achieves rapid and focal dehydration of the retinal tear margin by a process we call "photodehydration". Photocoagulation with the same wavelength at a higher power intensity is then performed in the dehydrated area to create the instantaneous fusion of retina with the RPE and choroid. This method for retinal reattachment repair without tamponade was then validated in the lensectomy/vitrectomy rabbit retinal detachment model.

Materials and Methods

All procedures were performed based on the provisions of the Australian National Health and Medical Research Council code of practice for the care and use of animals in research. They were approved by the St Vincent Hospital Animal Ethics Committee (ethics number 17-371AC). Human donor eyes were kindly donated from the Centre for Eye Research Australia Lions Eye Donation Service (LEDS) and approved by The Royal Victorian Eye and Ear Hospital (ethics number 13-1151H-007). Research on human donor tissue adhered to the Declaration of Helsinki.

Ex vivo *retinal detachment model*

Our *ex vivo* porcine model employed freshly harvested abattoir sourced porcine eyes (Diamond Valley, Laverton, VIC, Australia) maintained on ice for no more than 5 hours prior to use. In addition, human donor retinae were obtained from the Lions Eye Donation Service (Centre for Eye Research, East Melbourne, Vic, Australia) and used to validate the findings from porcine eyes. Human donor retina were retrieved and used for *ex vivo* experiment within 24 - 48 hours post-mortem. Porcine eyes were prepared by removing the anterior segment just behind the limbus using a scalpel blade followed by

the lens and then gentle aspiration of the vitreous using a 1 ml syringe (Terumo, Shibuya City, Tokyo, Japan). The anterior segment was already removed from human donor eyes. Four relaxing cuts were then made in the sclera and the eyecup was flattened. Any remaining vitreous was removed using a sponge tip (Weck-Cel, BVI Medical, Waltham, MA, USA). Using surgical scalpels (no22 Swann-Morton, Sheffield, UK) we prepared 6 mm x 12 mm fresh tissue blocks (**Figure 1**). Using cyanoacrylate glue (Loctite, Henkel Corporation, Westlake, OH) we secured the scleral surface of the tissue block to a plastic weigh tray (Proscitech, Kirwan, QLD, Australia) which was then placed under a dissection microscope (Stemi 1000, Zeiss, Oberkochen, Germany).

Tissue treatments: We treated one of the shorter edges (6 mm) of this tissue block to mimic repair of a retinal tear margin. The immediate integrity of the repair can be examined in several ways, (i) by introducing water under the retina to test if the seal was waterproof and (ii) pulling the retina tangentially and perpendicularly using a motorized micromanipulator (Zeiss, Oberkochen, Germany) to test adhesion strength. A tangential pull mimics the effect of the weight of the retina being pulled down by gravity on the tear repair margin or surface membrane contraction. Sample sizes of 5 repeats allows us to detect differences in retinal adhesion of 0.3 gm, with statistical power of 85%.

Specific treatment conditions

Control: The control condition consisted of no treatment, with tissue block allowed to rest for 3 minutes in ambient conditions (humidity 45-50% and temperature between 20-22^{o}C [XC4520 DHT11 Temperature and Humidity Sensor, Aosong Electronics Co. Ltd, Guangzhou, China]) prior to adhesion testing. In this condition, when the retina was pulled perpendicularly, the force represents the weight of the retina (and glue) as well as the bond between the retina and RPE. Resistance to tangential pulling represents the adhesion between the photoreceptor outer segments and the RPE. Because the tangential force is more clinically relevant we used that as our retinal adhesion parameter and as did the methods of Zauberman[6] in the cat and Yoon and Marmor in the rabbit.[7]

Photocoagulation alone: To model the current clinical approach, we compared the control condition to laser photocoagulation alone. In this case excess fluid was wicked away from the edge of the retina using a Weck-cell sponge point (BVI Medical, Waltham, MA, USA). Following wicking the 6 mm edge of the tissue block underwent standard laser photocoagulation. This was achieved by applying the retina edge laser burns using either an 810 nm (300 mW, 200 ms, Oculight SLx, Iridex, Mountainview, CA) or a 532 nm laser (200 mW power, 200 ms, Oculight TX, Iridex) through an 25G endoprobe (model number 14120, standard straight, Iridex). Between 60-80 burns were applied in two overlapping rows along the distal 6 mm edge of the tissue block to model in vivo repair of a retinal tear. Immediately after laser application approximately 200 μL of normal saline was slowly added under the retina around the non-lasered edges to minimize drag due to drying and compression by the scalpel incision. The retina was then pulled to test retinal adhesion strength, as detailed below.

Warm air retinal thermofusion: The retinal thermofusion approach was modelled by first dehydrating the edge of the tissue block for 1-3 minutes using two approaches. The first approach employed a custom-made device to deliver heated air (30 - 75^{o}C) at flow rates of 20-50 ml/min through a custom made 25G intraocular thin-walled flute (Ingeneus, Mount Waverley, VIC, Australia). Under a microscope, the handheld probe was manually manipulated to maintain the tip of the flute at approximately 1-3 mm from the surface of the retina. The probe was moved such that the edge of the retina was gradually dried (**please see Supplementary_Video1**). Comparisons of adhesion strength was made for 1, 2 or 3 minutes of warm air dehydration alone. Additionally, adhesion strength was quantified for 2 or 3 minutes of warm air dehydration followed by photocoagulation using an 810 nm laser, as described above. The relationship between adhesion force and temperature integral above basal tissue temperature (22.3±0.4^{o}C, T420, FLIR, Wilsonville, OR, USA) prior to photocoagulation was quantified. For both the control and no dehydration conditions this integral was close to zero.

Laser based retinal thermofusion: As a stream of air exiting the end of a narrow tube undergoes significant adiabatic expansion, a wide area of tissue can be affected, depending on the size of the tube and the speed of air flow. Thermodynamic modelling of 50 ml/min air flow through a 25G probe will impact a retina area some 5 mm in diameter (Supplementary Figure S1A). This approach has the potential to dry the retina away from the immediate region of the retinal tear. This was confirmed using thermal imaging in *ex vivo* porcine tissue (Supplementary Figure S1B). To achieve more focal dehydration of subretinal fluid, we explored the possibility of harnessing the physical properties of water whereby photons are absorbed directly to energize and disrupt water molecule bonds to liberate water molecules from the liquid phase. To achieve this, we employed lasers at wavelengths strongly and selectively absorbed by water to achieve more focal dehydration of retinal fluid. The absorbance spectra for water is shown in Supplementary Figure 2A, with distinct peaks at 1470 nm and 1940 nm.[20] We showed using 20 uL distilled water drops on glass slides that laser dehydration (using the 1470 nm laser) was more effective than air flow alone at removing water (Supplementary Figure S2B vs S2C). Laser liberated water can reform as small droplets near the main drop (Supplementary Figure S2C). We also showed that water was more efficiently dehydrated when the dehydration laser was combined with gentle airflow. This effect was dependent on the speed of air flow (Supplementary Figures S2D and S2E). Thereafter, subretinal fluid dehydration was achieved using targeted laser initially at 1470 nm (Anritsu, Kanagawa, Japan) mounted on a custom optical set up (MOGLabs Carlton VIC Australia) incorporating a diode aiming laser allowing coupling to a handheld 23G dual function endoprobe (23G soft-tip aspirating laser probe BL5293ASP, Bausch and Lomb, Bridgewater, NJ) so that the “aspirating” channel could be utilized for coaxial airflow to disperse the liberated water efficiently. The 1470 nm laser was superseded by a 1940 nm (high power diode, Akela Laser, Jamesburg, NJ) that was more strongly absorbed by water and had a greater range offering the potential to generate sufficient power for photocoagulation not just photodehydration. For that

prototype, the 1940 nm laser diode was incorporated into an existing laser chassis (eyeLase532, Ingeneus Pty Ltd. Mt Waverley, VIC Australia) for power supply, HeNe aiming low power visible red laser and output controls together with the fiberoptic (BL5293ASP, Bausch and Lomb) coupling. To further optimize the power delivery to the eye, a novel intraocular 25G dual bore handpiece (Ingeneus Pty Ltd. Mt Waverley, VIC Australia) was constructed using low–hydroxyl fiber for improved photon transmission efficiency.

Laser power was calibrated using a power meter (PM100D, Thorlabs, Newton, NJ) attached to either a S132C (700 to 1800 nm) or S148C (1200 to 2500 nm) sensor (Thorlabs). The 1470 nm and 1940 nm lasers were used to dry subretinal fluid at a power range of 15 – 45 mW and 5 – 15 mW, respectively. Immediately following dehydration, the margin of the retinal tear underwent photocoagulation using the 532 nm laser as described above. In addition, we considered whether the 1940 nm laser when used at a higher power could also be used as a photocoagulation laser. Thus, in several samples 1940 nm laser photodehydration was followed by 1940 nm photocoagulation (45-60 mW). We compared retinal adhesion achieved with this combination (1940 nm drying and coagulation) against 1940 nm laser photodehydration followed by 532 nm photocoagulation.

Ex vivo model outcome measures

Testing retinal adhesion strength: Using a small drop of cyanoacrylate glue (Loctite) the tip of an 8/0 suture (Vicryl Ethicon, Johnson and Johnson, New Brunswick. NJ) was attached to the surface of the retina, away from the retinal edge so as not to alter the retinal integrity, as shown in **Figure 1B**. The other end of the suture was attached to an isometric force transducer (MLT0402, ADInstruments, Sydney, NSW, Australia) connected via a pre-amplifier (FE232, ADInstruments) to a data acquisition system (Powerlab 8/SP, ADInstruments) with associated software (Chart, ADInstruments). The force transducer (MLT0402, ADInstruments) was attached to a motorized micromanipulator (Zeiss, Oberkochen, Germany) which allowed the attached suture and retina to be pulled laterally (to the right) away from the repair edge at a rate of 0.1 mm/second. This allowed us to quantify any increase in force from retinal adhesion to the underlying RPE and choroid following retinal treatment. Force data (100 samples/sec) were analyzed (Chart, ADInstruments, Bella Vista, NSW, Australia) by taking the peak force achieved during the controlled pull. The difference in peak force between experimental manipulations are compared.

Ex vivo Imaging and analysis: A color camera (XiQ, Ximea, Munster, Germany) was used to capture a video of the tissue surface throughout the experiment (**Figure 1B**). The tissue block was also imaged continuously using a thermal camera (T420, FLIR, Wilsonville, OR, USA) with a macro lens attached, which allowed us to quantify tissue temperature throughout the experiment (**Figure 1C**). Once the accuracy of the tissue temperature measurement using thermal imaging was confirmed by placing an implantable thermocouple probe (MLT1402 T-type fast thermocouple, ADInstruments)

placed under the edge of the retina. Thereafter, thermal imaging was used in preference because the thermocouple was unstable under the retinal sample and caused unwanted tissue distortion. Video sequences were acquired at a frame rate of 30 Hz and subsequently analyzed using FLIR tools (FLIR) to return the peak temperature and temperature integral. Temperature integral was determined by quantifying across the 6 x 12 mm retinal block the peak basal temperature. This basal temperature was averaged over one minute prior to any manipulation. The difference above basal temperature was quantified for each second and then summed over the full duration of retina dehydration (sum ^{o}C x sec). The relationship between tissue temperature integral during dehydration (i.e. prior to photocoagulation) and peak adhesion force was examined.

Quantifying change in tissue thickness: Finally, the left most (distal) edge of the tissue block was also imaged using optical coherence tomography (Bioptigen with 18 mm lens attached, Leica, Wetzlar, Germany) as shown in **Figures 1A and 1B** (scan direction). This enabled us to quantify change in tissue thickness and subretinal fluid. Imaging (5 frames per second) was undertaken with a 3 mm B-scan (500 A-scans) oriented along from left to right. This scan positioning captured the edge of the retina, the underlying RPE and sclera, the fluid meniscus and any subretinal fluid as shown in **Figure 1A**. Analysis was undertaken by measuring tissue thickness for the inner limiting membrane to the RPE. Measurements were made perpendicular to the RPE every 20 μm from the edge of the retina and at every 15 seconds from the onset of dehydration. To consider the effect of dehydration, thickness measurements for a given sample were expressed relative as a % relative to its own baseline thickness.

In vivo rabbit model of retinal detachment

Twenty pigmented, Dutch-belted adult rabbits weighing at least 3 kg underwent the full surgical sequence in this study. First, the 1470 nm laser with airflow was used for drying the retinal tissue and 532 nm laser for photocoagulation (6 animals), this was replaced with the longer wavelength 1940 nm laser (5 animals) and finally the 1940 nm laser was used for both drying and photocoagulation of the retina (6 animals).

Animals were premedicated via an intramuscular injection with a non-steroidal anti-inflammatory agent (Caprieve at 1.5mg/kg final dose, Norbrook, Newry, UK) 15 minutes prior to anaesthesia, at which time pupils were dilated using one drop of atropine (1%, Alcon, Geneva, Switzerland), tropicamide (1%, Alcon) and phenylephrine (10%, Alcon). Induction of anaesthesia was undertaken via an intramuscular injection of a combination of ketamine (35 mg/kg Troy Laboratories, Glendenning, NSW, Australia) and xylazine (5 mg/kg Troy Laboratories). Animals were then maintained using 1-1.5% isoflurane (Isoflo, Zoetis, Parsippany, NJ, USA) delivered with oxygen at a flow rate of 2 ml/min. Depth of anaesthesia was ensured prior to surgery. Pulse, respiration, and anaesthesia depth were monitored throughout surgery.

Surgical technique: Key steps related to model induction are summarised in **Figure 2**. In brief, rabbits were positioned on their right side on a warming pad under the operating microscope and a lid speculum was inserted. To prevent dislocation of the speculum, 3/0 silk suture (Johnson and Johnson, New Brunswick, NJ, USA) was passed through the superior and inferior eyelids to secure the arms of the speculum and the nictitating membrane was also sutured to prevent migration during surgery. Localised conjunctival peritomies were created and a 25G cannula (Alcon Constellation system, Fort Worth, TX, USA) was secured with 8/0 Vicryl (Johnson and Johnson) to the sclera for the infusion. Without securing the cannula, the weight of the infusion line can dislodge the cannula as the rabbit sclera is much thinner than human eyes, for which the cannula system was designed. The rabbit eye has virtually no pars plana for safe placement of the sclerotomies to avoid the peripheral retina and in several preliminary surgeries a peripheral retinal defect developed due to the Fragmatome ultrasonic action resulting in retinal detachment. Thus, a near perpendicular trans-limbal insertion of the 25G cannulas through the iris root into the vitreous cavity was adopted. Adrenaline (1 ug/ml final concentration, Aspen Medicals) and low molecular weight heparin (Enoxaparin, 20 units/ml, Sanofi-Aventis, Paris, France) was added to the balanced salt solution (BSS, Alcon) intraocular infusion. The heparin minimises fibrin formation[5, 21] and the adrenalin both aids stable pupil dilation and also helped to reduce any heparin induced bleeding.

A lensectomy was essential for adequate clearance of the anterior vitreous to allow placement of the detachment bleb anteriorly so that it was high enough to remain above any pooling fluid during the dehydration phase of the retinopexy, and also to avoid the “tear drop” effect from residual vitreous on the posterior lens capsule after the fluid gas exchange preventing visualization of the retinal defect margin to enable the RTF treatment to be performed. A limbal clear corneal incision was made (Clearcut S keratome blade, Alcon) to perform the 25G phacoemulsification lensectomy (Infinity Ozil, Alcon). After completion of the lensectomy, a 10/0 monofilament nylon suture (Johnson and Johnson) was used to close the corneal wound. Two more 25G trocars with cannulas were passed through the iris root into the vitreous cavity in the superior quadrants and the cannulas were secured to the sclera using 8/0 Vicryl sutures.

For visualization of the retina, a Landers wide field vitrectomy system supporting arm was attached to the operating microscope and a Peyman–Wessels–Landers (PWL) lens (Ocular Instruments, Bellevue, WA, USA) was placed above the cornea. The 25G vitrector and light pipe were inserted, any residual lens capsule was cleared and then all accessible vitreous gel was removed. To ensure that as much gel as possible was removed, triamcinolone (TA, 0.1 ml, Kenacort-40 Aspen Medical, Canberra, Australia) was repeatedly injected into the vitreous cavity to aid visualization of the clear vitreous.[22] and ensure there was as complete removal of vitreous as possible. The vitreous was more firmly attached over the medullary wing than elsewhere and the peripheral vitreous fibrillar density was much less in the periphery consistent with previous anatomical studies. [23] An attempt to

create a posterior detachment was made in all cases but not completely convincingly in all cases in this rabbit model. In one case a small retinal tear developed at the border of the medullary rays causing a localized detachment and surgery was abandoned. When there was no obvious release (as seen in human surgery) after multiple high vacuum aspiration attempts, high vacuum aspiration was performed extensively after repeat TA injection over wide areas of the peripheral retina. There was no difference in the post-operative course of those animals where there were no intraoperative tears.

To create the retinal detachment, BSS (Alcon) was injected into the subretinal space through a soft-tipped 25G cannula (Alcon) attached to a syringe controlled by an assistant. The soft-tipped cannula was placed on the retinal surface as the BSS injection commenced and the injection was maintained until an adequate area of detachment formed. The localized bleb of retinal detachment was created as anteriorly as possible in the mid periphery of the inferior retina so that it remained above any re-accumulating fluid and could be kept dry. The vitrector was used to create a retinal defect (2-3 mm diameter) to mimic retinal tears found during retinal detachment surgery. A standard fluid-gas exchange with aspirating 25G soft-tipped cannula through the retinal defect was performed, as in traditional vitreoretinal surgery.

Once the retinal tear margin and the retina was “reattached” - as per routine surgical criteria - dehydration of a 1–2 mm retinal zone around the tear margin was then achieved with the combination of laser (initially with the 1470 nm prototype and subsequently with the 1940 nm unit) and an airstream delivered via the aspirating channel of a 25G aspirating laser handpiece (25G soft-tip aspirating laser probe BL5293ASP, Bausch and Lomb) with the aid of an aiming beam. The airflow was generated by an independent syringe pump (22, Harvard Apparatus, Holliston, MA) connected through a fine syringe filter (0.22 μm, Millex GV, Merck Millipore, Burlington, MA). The airflow was controlled between 20 - 40 ml/min by the assistant. The intraocular pressure (IOP) was not affected due to the regulation of IOP by the Constellation console vented gas forced infusion (VGFI) control system. The laser for photodehydration was used at power of 15 – 45 mW for the 1470 nm and 5 - 15 mW for the 1940 nm and drying took between 3-5 minutes. Adequate dehydration was judged when the sheen from the fluid meniscus where the retinal margin joined the exposed RPE layer was lost, the adjacent retinal surface developed a matte reflex and the dehydrated retina appeared darker and thinner than the adjacent untreated retina.

Due to the formation of copious plasmoid aqueous by the rabbit eye,[24] the retinal defect was sometimes flooded by this fluid thus preventing subretinal space dehydration. In addition, sometimes the laser probe became adherent to it and movement displaced the retinal edge. To counter this, we modified our technique to incorporate a chandelier fibreoptic light (25G, W/RFID 8065751577, Alcon) so that with a bimanual technique concurrent continuous aspiration (25G soft tip) within the retinal tear was performed during the laser dehydration and subsequent photocoagulation.

Once adequate dehydration was achieved, two to three continuous rows of 500 ms duration laser pulses using a 532 nm (Iridex) laser with a spot size of approximately 500 µm set at 500 ms duration delivered via a 25G laser fibreoptic (BL5293ASP, Bausch and Lomb) was applied around the tear margin. The intensity was set at levels sufficient to produce opacification of the treated retina (150 – 250 mW pulsed). A similar effect could be achieved using the 1940 nm set at higher power (45 – 60 mW, continuous). In 3 rabbits (1 that was lasered only and 2 that had undergone the RTF procedure) 10/0 suture secured to the retina below the inferior tear margin using fibrin glue (Fibrin Sealant, Baxter, Deerfield, IL). As above, this suture was attached to an isometric force transducer (MLT0402, ADInstruments) and using a motorized micromanipulator (Zeiss) constant force was applied over 90-120 seconds to test adhesion strength. Animals were killed at the end of the adhesion test.

In the remaining 17 rabbits, BSS infusion was then slowly recommenced to fill the vitreous cavity. The sclerotomies were closed with an 10/0 Nylon monofilament suture (Ethicon, Johnson and Johnson) and exposed cut suture ends were rounded off using the 532 nm laser to soften the cut ends. These animals were followed for 14 days.

Post-surgery: Following surgery animals received 5 ml of warmed Hartman's solution subcutaneously (Baxter, Deerfield, IL, USA) and kept warm until they regain the righting reflex. Once awake and over the first day, animals were encouraged to drink (hand feed using a 50 ml syringe if necessary) and eat softened food pellets. Post-surgical care of eyes consisted of mydriatic (once a day 1% atropine, Alcon), Prednefrin Forte (Allergan, Dublin, Ireland, 4 times per day) and antibiotic ointment (4 times per day 1% Chlorsig, Aspen Pharma, St Leonard, NSW, Australia). Additional subcutaneous warmed Hartman's solution was given if there were any signs of dehydration. Caprieve (Norbrook, Newry, UK) was given once a day if animals showed any signs of pain.

Two weeks after surgery animals were deeply anesthetised (intramuscular ketamine 35 mg/kg and xylazine 5 mg/kg mixture) and images of the retina taken using a fundus camera (Micron III, Pheonix, Pleasanton, CA). Immediately following imaging animals were killed (intravenous 100 mg/kg lethabarb, Virbac, Milperra NSW, Australia). Once eyes were enucleated, 100 µL of Davidsons's fixative was injected into the eye using a 30G needle through the cornea. The eye was then immersed in Davidson's fixative for between 16- 24 hours. Eyes were then dissected and processed for paraffin embedding (Melbourne Histology Platform, Parkville, VIC, Australia). Ten-micron thick sections were cut through the treated area and stained for Haematoxylin and Eosin (Sigma, St Louis, MO, USA). Images were captured using 2x 0.05 NA or 10x 0.40 NA objective on an BX51 brightfield microscope (Olympus, Tokyo, Japan) at the Microscope Facility at The Florey Institute of Neuroscience and Mental (Melbourne Victoria Australia). Outcome measures were *in vivo* fundus imaging and histological confirmation that the retinal repair remained intact after 14 days.

Statistical analyses

Data are given as group mean (± standard error of the mean). Comparisons between conditions were made using one way ANOVA, with Dunnett's multiple comparisons between groups (Prism 9, Graphpad, San Diego, CA, USA).

Results

Ex-vivo retinal detachment model

Figure 3 show that warm air (50-70^{o}C) at rates between 20-70 ml/min change the appearance of ex vivo porcine retina on OCT. After 3 minutes of dehydration there was less evidence of subretinal fluid, retinal thinning, increased reflectivity at the level of the RPE and inner limiting membrane and overall, a more homogenous retinal appearance. Quantification of retinal thickness at the edge of the repair, confirms that the largest effect occurred nearest the retinal margin. Overall, the retina was significantly thinned (time effect on 2-way ANOVA, $p<0.001$); specifically, by 16% (±3%) after 3 minutes.

Next, we considered the effect of retinal thermofusion on adhesion achieved between the retina and underlying RPE/choroid (Figure 4A). Following treatment, on the left edge of the retinal section, cyanoacrylate glue was applied near the midpoint of the retina and a fiber connecting the retina to the force transducer was attached (Figure 4A). Figure 4B shows example of force traces during a controlled pull toward the right, away from the retinal repair edge. Compared with photocoagulation alone, retinal thermofusion using warmed air dehydration prior to photocoagulation using an 810 nm laser produced higher adhesion force (Figure 4B). Note that forces above 2 g often (~80% of cases) exceeded the strength of the post-mortem porcine retina. Such forces resulted in the untreated retina tearing from the RTF treated zone. The peak force in those instances thus underestimates the separation force of the RTF bond itself. Due to the nature of cyanoacrylate chain-polymerization (exothermic and can release formaldehyde[25, 26]) gluing a fiber over the thermofusion bond area would distort the retinal strength, as such no attempts were made to measure the attachment strength directly. Nevertheless, the peak force was used here as a surrogate for repair adhesion strength as summarised in Figure 4C. Photocoagulation alone did not significantly increase adhesion compared with untreated samples (one-way ANOVA, multiple comparison, $p = 0.98$). Dehydration for 2 or 3 minutes (1 min $p = 0.86$, 2 min $p = 0.01$, 3 min $p = 0.0008$) as well as RTF with dehydration for 2 minutes ($p = 0.0016$) or 3 minutes ($p < 0.0001$) all produced significantly higher adhesion. Figure 4D, shows that the strength of adhesion increased with higher temperature integrals achieved during the dehydration process, with data for dehydration alone as well as for RTF (drying followed by photocoagulation) both following a similar relationship. Although the warm air achieved SRF dehydration and facilitated strong bond formation (Figure 4), the thermal footprint of warm air dehydration was very much greater than the diameter of the delivering tube due to adiabatic

expansion of moving air out of a small aperture (please see Supplementary Figures S1A and S1B**)** and has the potential to damage the retina well beyond the immediate zone of dehydration. This would be clinically unacceptable. A novel approach to dehydrating the subretinal space that limits the thermal footprint (Figure S1C) was to use lasers tuned to wavelengths targeting key water absorption peaks (Figure S2A). Figure S2 also shows that more effective dehydration was achieved when laser dehydration was used in combination with airflow (Figures S1D and S1E).

Figure 5A show that when used in combination with low airflow (20 ml/min) dehydration using 1470 nm or 1970 nm lasers produced similar retinal adhesion forces (one-way ANOVA $p = 0.95$). When dehydration was followed by photocoagulation retinal adhesion force was consistently higher than with laser dehydration alone (two-way ANOVA, interaction $p = 0.92$, type of treatment $p = 0.64$, photocoagulation effect $p = 0.0045$). As some early experiments employed 810 nm photocoagulation (due to the availability of that laser in the laboratory), whereas later experiments employed 532 nm photocoagulation we compared these directly. Figure 5B shows that 810 and 532 nm laser photocoagulation bonding effect were not different (t-test, $p = 0.24$) and can thus be used interchangeably for photocoagulation.

Once we had established our *ex vivo* retinal detachment model, we wanted to ensure that our observations on porcine specimen were also relevant to human retina tissue. We quantified adhesion force achieved using the 1940 nm laser for tissue photodehydration followed by 532 nm or 1940 nm laser photocoagulation in porcine or human retinal samples (Figure 6B and 6C respectively). Photodehydration alone produced greater adhesion strength than controls (Figure 6C). RTF produced stronger adhesion than drying alone. In human tissues RTF resulted in significantly stronger adhesion than untreated samples (Figure 6D). Comparisons of photocoagulating lasers showed that for both porcine (Figure 6C, $p = 0.49$) and human (Figure 6D, $p = 0.99$) tissue there was no difference between the 532 nm or 1940 nm lasers that were applied after 1940 nm drying.

In three rabbits we assessed retinal adhesion strength *in vivo.* It proved to be particularly challenging gluing the suture to the retinal tear margin as cyanoacrylate released formaldehyde[27] causing corneal opacification. After some trial and error, we were successful when the cyanoacrylate was replaced with a fibrin glue which produces a natural adhesive relying on the formation of a fibrin clot to firmly hold the suture in place. Figure 7A shows three adhesion force traces obtained from RTF using 1470 nm laser for photodehydration and 532 nm laser for coagulation. The force required to pull the retina away from the choroid was above 2 g which was greater than that of *ex vivo* baseline force of 0.5 g (Figure 7A).

Clinically, the strength of retinal adhesion is in itself not important (formation of an effective waterproof seal is the priority) for the majority of cases during retinal detachment repair but retinal slippage during giant retinal tear repair remains a significant surgical challenge[28] despite the introduction of

perfluorinated liquids (PFCL) to re-position the retina. To assess whether the RTF method could prevent GRT slippage in a PFCL filled eye, we first measured *ex vivo* the transmission of 1940 nm light through PFCL (Okta-line perfluoro-octane liquid, Bausch and Lomb, Berlin, Germany), and showed that whereas water allowed 1.1 ±0.9% transmission, PFCL allowed 87% transmission of the 1940 nm laser. We then created a GRT model by placing a 6x12mm strip of porcine retina inside a well (Fig S4A) to hold the tissue block vertical after which a microfiber was glued to the retinal surface (as per the previous testing). When compared with an untreated upper retinal edge, RTF either in air or with the laser probe and retinal block submerged both produce significant increases in adhesion force (Fig S4B, one-way ANOVA, $p = 0.04$). There was no difference between the two approaches in terms of resultant force (post-hoc, $p = 0.42$).

Longer term surgery outcome of RTF repair in a rabbit model

Initially, we used the 1470 nm laser for drying followed by the standard 532 nm clinical laser for photocoagulation (6 surgeries). The 1940 nm laser subsequently replaced the 1470 nm laser for drying and then further refined to using the same laser at 1940 nm for both tissue photodehydration and coagulation in the final surgical protocol. Animals were monitored for at least two weeks post-surgery at which fundus photographs were used to assess whether the retina remained intact before enucleating the eye for histological processing and further confirmation. Figure 7B summarises uncomplicated, completed surgeries for the different surgical approaches. For 1470 nm laser photodehydration followed by 532 nm laser photocoagulation, four retinal repairs were still attached, however in two surgeries retinae were detached at the endpoint. For RTF surgery utilising 1940 nm laser for photodehydration followed by coagulation using 532 nm or 1940 nm lasers, repair was successful in all cases at the endpoint, as determined by fundus imaging and histology (Figure 8 is representative of two surgeries with remaining histology in supplementary S3). Hematoxylin and Eosin staining of the tissue showed an obvious loss of the retinal architecture and therefore thinning at the RTF repair site due to the thermal effect of the 1940 nm laser and importantly fusion of the retina to the RPE and choroid as indicated by the lack of subretinal space (coloured arrows) unlike the non-dehydrated retina region adjacent to the site of repair. At the edge of the RTF repair site where no surgery was performed there was a transition to normal retina whereby retinal layers were easily distinguished. Supplementary Figure S5 suggests that this transition zone is less than 1 mm. Retinal thickness measurements show no significant differences in retinal thickness for any region away from the repair edge, suggesting that gross retinal structure was largely unaffected.

Discussion

Sealing all retinal tears is the essential surgical step to treat a rhegmatogenous retinal detachment. Since Gonin developed his “igni-puncture” method utilizing a thermal injury to both the retina and the adjacent RPE/choroid[2-4], it has not been possible to reliably cure detachments

intraoperatively without some form of support holding both injured layers together while the wound healing process occurs. A method that is independent of a wound healing response to create an immediate seal that is independent of the tear location would eliminate the need to support the retina with a tamponade agent, either as gas or liquid, thus restoring vision quickly, enabling earlier return to normal activities, including air travel, much earlier, with potentially better quality of vision. Once the subretinal space is isolated intraoperatively, the vitreous cavity can be refilled with BSS[29] at the end of the retinopexy and allow the physiological mechanisms of subretinal fluid removal [30] for retinal reattachment to occur in a similar manner to pneumatic retinopexy. This should offer similar potential benefits to pneumatic retinopexy when compared with vitrectomy: a lower risk of retinal displacement[31-34], retinal folds[35, 36] and disruption to the outer retina as evidence by discontinuity of the ellipsoid zone and external limiting membrane as seen with OCT[16, 37]

Consistent with a previous study[18] we show that RTF can histologically bond the retina and underlying RPE and choroid instantaneously in a rabbit retinal detachment model (Figure 8), producing immediate and strong adhesion of the retina to the underlying RPE and choroid. Functional demonstrations of immediate and strong adhesion were also made using using *ex vivo* porcine tissue (Figure 4), human tissue (Figure 6) as well as *in vivo* in rabbit eyes (Figure 7A). Moreover, we were able to show enduring adhesion throughout a 2 week follow up period using the *in vivo* rabbit retinal detachment model.

The key clinical finding was that a short preliminary step of subretinal space dehydration at the retinal tear margin allows both tissues to be in contact at the time of coagulation, resulting in fusion of the retina to underlying RPE and choroid and creates an immediate and strong adhesion. Furthermore, we show that RTF can be achieved by targeting energy absorption peaks at 1470 nm or 1940 nm to agitate and release water molecules in situ from the liquid phase to vapour. When coupled with low air flow (10-20 ml/min) this approach was effective at removing SRF allowing for photocoagulation to produce an immediate adhesion between the retina and underlying RPE and choroid. The addition of low air flow at room temperature increased the speed of dehydration whilst avoiding excessive drying of adjacent retinal areas associated with adiabatic expansion of high speed (50-70 ml/min) warm air and prevented potential elevation of intraocular temperature that can enhance retinal damage.[38]

Retinal attachment force determination

To test the efficiency of a variety of dehydration methods we developed an *ex vivo* full thickness retina/RPE/choroid/sclera model broadly based on the method of Yoon and Marmor[7] and Zauberman[6]. Here we show the porcine eye tissue provides a robust model for human tissue, showing dehydration and coagulation characteristics as well as adhesion forces that were comparable with human tissue.

Retinal adhesion to the underlying RPE and choroid was measured using the same standardized explant preparation (see Methods). This is the first documentation of retinal adhesion strength immediately following laser photocoagulation. Yoon and Marmor[7] created a bleb of retinal detachment, allowed it to spontaneously reattach and then treated both the reattached retina and non-detached (control) retina. They found that the attachment was only 50% of normal at 8 hours rising to twice normal after 3 days but they did not measure adhesion immediately after laser treatment.

Zauberman[6] assessed the adhesion strength post photocoagulation, diathermy and cryopexy in the cat eye using a similar methodology to ours but assessed the adhesion strength between 2 and 96 days after treatment. They found that the adhesion over the tapetum lucidum ranged from 15 - 40 mg at day 2, rising to 65 - 155 mg at day 7 with a maximum of 185 – 365 mg from day 21 onwards. No measurements were made immediately after the treatment.

Over the course of 3 minutes of dehydration the retina thinned by 20% (Figure 3), with regions nearer the retinal edge showing the most thinning. The fluid meniscus at the retinal edge and exposed RPE interface was also monitored and was noteworthy because the meniscus reformed after the initial drying passes presumably as more peripheral SRF was drawn to the exposed retinal edge. This continued until the more distal retina had also dehydrated. This phenomenon was also noted *in vivo* during the rabbit eye detachment surgery. Several clinical indicators proved reliable indirect markers of adequate subretinal space drying; removal of the fluid meniscus dark band at the retinal defect edge, thinning of the retinal edge creating a distinct step down from the adjacent untreated retina, loss of surface reflectivity (glistening) from the hydrated retina or RPE surface and the development of a matt subtly stippled “sheen” as the retinal surface dried. These metrics were used successfully to judge adequate dehydration prior to coagulation.

We show that immediate adhesion force achieved was related to the tissue temperature integral (temperature x time) achieved using the dehydration phase (Figure 4D), with drying for longer durations producing stronger immediate adhesion. We interpret these observations to be due to dehydration of glycoproteins located on both retinal photoreceptors and RPE[39, 40] cell membranes, thus reducing their lubrication effect[41]. Critically, this increased adhesion from drying alone could be rapidly reversed with rehydration and does not create a clinically useful retinopexy adhesion. We believe that the ready slippage of the retina during giant retinal tear repair or with macula translocation after macula detachment occurs because the SRF hydrates glycoproteins and increases their lubricious quality.

***In vivo* rabbit eye surgery**

In vivo laser photodehydration with coaxial airflow resulted in more targeted dehydration largely confined to the laser footprint. This is because the release of water molecules from the water phase (evaporation) is primarily due to the photons energizing the water molecular bonds. The low rate of

airflow (10-20 ml/min) helped to disperse the laser liberated water molecules faster than without any coaxial flow (Figure S2) without the risk of retinal edge elevation as can occur with more forceful airflow. Importantly there was no observable retinal surface dehydration nor other adverse effects beyond the laser exposed area - in distinct contrast to the effect created by the warm air dehydration method (Figure S1A). We believe this to be because the evaporation effect is primarily due to the photic disruption of the water-water bonds in the liquid phase with the airflow being just enough to disperse the vapor. As with traditional photocoagulation, slow continuous movements ("painting") around the retinal defect margin are performed for 2-3 minutes during which the retinal surface at the defect edge becomes thinner, and the margin appears darker (choroidal pigment was more visible through the thinner retina) and develops a matt/slightly speckled appearance to match the matt appearance of the dried exposed RPE within the defect (see Supplementary Video 4). Initially the base of the retinal defect edge in contact with the RPE has a persistent glistening from the fluid meniscus. Even after the meniscus is minimized it can reform because residual SRF is recruited from the surrounding areas until prevented by sufficient retinal dehydration of the area surrounding the tear. The clinical judgment of adequate retinal dehydration prior to using higher power to photocoagulate will be a critical skill to acquire.

It is important to recognize that evaporation of the meniscus was best achieved by aiming the laser/airflow directly at the meniscus at the RPE/ retinal tear edge because the evaporation effect is primarily the photon stream. If the meniscus is in "shadow" it will be underexposed to the photons and not efficiently evaporated.

The laser power output, spot size and speed of moving the fiberoptic tip during the dehydration was visually monitored during the dehydration so that there was no retinal opacification which would indicate a temperature elevation towards the coagulation range. The laser beam is mildly divergent leaving the fiberoptic tip, as such laser power density varies with the distance between handpiece tip and retina as with a traditional 532 nm or 810 nm laser fibreoptic delivery. The 1940 nm co-axial probe we developed delivers sufficient power to coagulate the retina and RPE but utilizes water molecules as the chromophore rather than melanin or haemoglobin. This effect is not dependent on dehydration of the subretinal space so that the laser can be used – with or without the airflow - to photocoagulate other areas of retina for prophylactic laser or to treat tears in attached retina. However, as the laser energy is absorbed by water this wavelength cannot be used to treat the retina when delivered though the cornea or via an indirect ophthalmoscope nor via a fibreoptic in the presence of vitreous.

The retinal thermofusion method achieves at vitrectomy, the effect of pneumatic retinopexy obstructing access of liquid vitreous to the SRS but does so irrespective of the tear location (and presumably the length). As such, it offers the potential to facilitate macular reattachment as the outer retinal oedema is diminishing[36] and achieve the same potential quality of vision benefits documented in the PIVOT study and reduction of the incidence of outer retinal folds[35]. One of the most important

potential benefits of 1940 nm laser based RTF is the immediate adhesion formation along a giant retinal tear prior to the removal of the PFCL thus preventing retinal slippage after PFCL removal and eliminate the need for longer term tamponade and potential second surgery.[1, 42] Allowing the retina to reattach naturally via RPE pumps may result in better vision outcomes.[16, 35, 36]

The laser-based RTF method to encircle a retinal tear margin with laser is an intuitive manipulation for trained retinal surgeons. The purpose built 25g coaxial fibreoptic with the high transmission of near infrared light by the low-hydroxy fiber ensures that the one handpiece can be used for both photodehydration and photocoagulation thus minimizing the exchange of instruments and reducing the surgery time.

In conclusion, the insertion of a short preliminary step of photodehydration prior to laser photocoagulation enables formation of a strong immediate attachment of the retina to the underlying RPE and choroid in the retinal detachment rabbit model. The creation of an immediate and stable intraoperative retinopexy seal should enable retinal detachment repair without tamponade irrespective of the retinal tear or relaxing retinotomy location and significantly reduce the need for liquid tamponade and the second procedure for its removal. Should the retinal thermofusion technique prove beneficial in a clinical trail, it may be a significant step forward for the field.

Acknowledgements

We would like to acknowledge full funding support from the Department of Defense office of the Congressionally Directed Medical Research Programs (CDMRP) under the Vision Research Program, Technology/Therapeutic Development Award (W81XWH-15-VRP-TTDA). The authors would also like to thank Professor Robert Scholten and Dr Sebastian Saliba from Moglabs (Carlton, Australia) for their invaluable support and expertise with laser systems.

References:

1. Wong D, Williams RL, German MJ. Exchange of perfluorodecalin for gas or oil: a model for avoiding slippage. Graefes Arch Clin Exp Ophthalmol 1998;236(3):234-7.
2. Rumpf J. Jules Gonin. Inventor of the surgical treatment for retinal detachment. Survey of Ophthalmology 1976;21(3):276-84.
3. Wolfensberger T. Jules gonin. Pioneer of retinal detachment surgery. Indian Journal of Ophthalmology 2003;51(4):303-8.
4. Gonin J. La pathogénie du décollement spontané de la rétine. Ann d'Ocullist (Paris) 1904;132(1):30-55.
5. Johnson R, Irvine A, Wood I. Endolaser, cryopexy, and retinal reattachment in the air-filled eye: a clinicopathologic correlation. Archives of Ophthalmology 1987;105(2):231-4.
6. Zauberman H. Tensile strength of chorioretinal lesions produced by photocoagulation, diathermy, and cryopexy. The British Journal of Ophthalmology 1969;53(11):749-52.
7. Yoon Y, Marmor M. Rapid enhancement of retinal adhesion by laser photocoagulation. Ophthalmology 1988;95(10):1385-8.
8. Vaziri K, Schwartz SG, Kishor KS, Flynn HW, Jr. Tamponade in the surgical management of retinal detachment. Clinical ophthalmology (Auckland, NZ) 2016;10:471-6.
9. Schwartz SG, Flynn HW. Primary retinal detachment: scleral buckle or pars plana vitrectomy? Curr Opin Ophthalmol 2006;17(3):245-50.
10. Vaziri K, Schwartz SG, Kishor KS, Flynn HW, Jr. Tamponade in the surgical management of retinal detachment. Clin Ophthalmol 2016;10:471-6.
11. Silvanus M-T, Moldzio P, Bornfeld N, Peters J. Visual loss following intraocular gas injection. Deutsches Arzteblatt international 2008;105(6):108-12.
12. Butler WP, Steinkraus LW, Burlingame EE, et al. Clinical Impact of Cabin Altitude Restriction Following Aeromedical Evacuation. Military Medicine 2018;183(suppl_1):193-202.
13. Fang IM, Huang J-S. Central retinal artery occlusion caused by expansion of intraocular gas at high altitude. American Journal of Ophthalmology 2002;134(4):603-5.
14. Foulsham W, Chen XN, Vavvas DG. ALTITUDE-ASSOCIATED INTRAOCULAR PRESSURE CHANGES IN A GAS-FILLED EYE. Retinal cases & brief reports 2019:10.1097/ICB.0000000000000852.
15. Miller JB, Papakostas TD, Vavvas DG. Complications of emulsified silicone oil after retinal detachment repair. Semin Ophthalmol 2014;29(5-6):312-8.
16. Muni RH, Felfeli T, Sadda SR, et al. Postoperative Photoreceptor Integrity Following Pneumatic Retinopexy vs Pars Plana Vitrectomy for Retinal Detachment Repair: A Post Hoc Optical Coherence Tomography Analysis From the Pneumatic Retinopexy Versus Vitrectomy for the Management of Primary Rhegmatogenous Retinal Detachment Outcomes Randomized Trial. JAMA Ophthalmol 2021;139(6):620-7.
17. Martinez-Castillo V, Zapata MA, Boixadera A, et al. Pars plana vitrectomy, laser retinopexy, and aqueous tamponade for pseudophakic rhegmatogenous retinal detachment. Ophthalmology 2007;114(2):297-302.
18. Heriot W. Thermofusion of the retina with the RPE to seal tears during retinal detachment repair. Graefe's Archives for Clinical & Experimental Ophthalmology 2016;254(4):691-6.
19. Stappler T, Williams R, Gibran S, et al. A guide to the removal of heavy silicone oil. Br J Ophthalmol 2008;92(6):844-7.
20. Bertie JE, Lan Z. Infrared Intensities of Liquids XX: The Intensity of the OH Stretching Band of Liquid Water Revisited, and the Best Current Values of the Optical Constants of H2O(l) at 25°C between 15,000 and 1 cm-1. Applied Spectroscopy 1996;50(8):1047-57.
21. Zarei R, Azimi R, Moghimi S, et al. Inhibition of intraocular fibrin formation after infusion of low-molecular-weight heparin during combined phacoemulsification-trabeculectomy surgery. Journal of Cataract & Refractive Surgery 2006;32(11):1921-5.
22. Sakamoto T, Ishibashi T. Visualizing vitreous in vitrectomy by triamcinolone. Graefe's Archive for Clinical and Experimental Ophthalmology 2009;247(9):1153-63.

654 23. Los LI, van Luyn MJ, Nieuwenhuis P. Organization of the rabbit vitreous body: lamellae,
655 Cloquet's channel and a novel structure, the 'alae canalis Cloqueti'. Exp Eye Res 1999;69(3):343-50.
656 24. Al-Nawaiseh S, Thieltges F, Liu Z, et al. A Step by Step Protocol for Subretinal Surgery in
657 Rabbits. J Vis Exp 2016(115).
658 25. Chen S-N, Hwang J-F, Tseng L-F, Lin C-J. Subthreshold diode micropulse photocoagulation
659 for the treatment of chronic central serous chorioretinopathy with juxtafoveal leakage. Ophthalmology
660 2008;115(12):2229-34.
661 26. Leggat PA, Smith DR, Kedjarune U. SURGICAL APPLICATIONS OF CYANOACRYLATE
662 ADHESIVES: A REVIEW OF TOXICITY. ANZ Journal of Surgery 2007;77(4):209-13.
663 27. Tseng Y-C, Tabata Y, Hyon S-H, Ikada Y. In vitro toxicity test of 2-cyanoacrylate polymers by
664 cell culture method. Journal of Biomedical Materials Research 1990;24(10):1355-67.
665 28. Sirimaharaj M, Balachandran C, Chan WC, et al. Vitrectomy with short term postoperative
666 tamponade using perfluorocarbon liquid for giant retinal tears. Br J Ophthalmol 2005;89(9):1176-9.
667 29. Martínez-Castillo V, Zapata M, Boixadera A, et al. Pars plana vitrectomy, laser retinopexy, and
668 aqueous tamponade for pseudophakic rhegmatogenous retinal detachment. Ophthalmology
669 2007;114(2):297-302.
670 30. Marmor MF. Control of subretinal fluid: Experimental and clinical studies. Eye 1990;4(2):340-
671 4.
672 31. Shiragami C, Shiraga F, Yamaji H, et al. Unintentional Displacement of the Retina after
673 Standard Vitrectomy for Rhegmatogenous Retinal Detachment. Ophthalmology 2010;117(1):86-
674 92.e1.
675 32. Brosh K, Francisconi CLM, Qian J, et al. Retinal Displacement Following Pneumatic
676 Retinopexy vs Pars Plana Vitrectomy for Rhegmatogenous Retinal Detachment. JAMA
677 Ophthalmology 2020.
678 33. Francisconi CLM, Marafon SB, Figueiredo NA, et al. Retinal Displacement after Pneumatic
679 Retinopexy versus Vitrectomy for Rhegmatogenous Retinal Detachment (ALIGN). Ophthalmology
680 2022;129(4):458-61.
681 34. Hillier RJ, Felfeli T, Berger AR, et al. The Pneumatic Retinopexy versus Vitrectomy for the
682 Management of Primary Rhegmatogenous Retinal Detachment Outcomes Randomized Trial (PIVOT).
683 Ophthalmology 2019;126(4):531-9.
684 35. Lee WW, Bansal A, Sadda SR, et al. Outer Retinal Folds after Pars Plana Vitrectomy vs.
685 Pneumatic Retinopexy for Retinal Detachment Repair: Post hoc analysis from PIVOT. Ophthalmol
686 Retina 2022;6(3):234-42.
687 36. Bansal A, Lee WW, Felfeli T, Muni RH. Real-Time In Vivo Assessment of Retinal
688 Reattachment in Humans Using Swept-Source Optical Coherence Tomography. American Journal of
689 Ophthalmology 2021;227:265-74.
690 37. Farahvash A, Marafon SB, Juncal VR, et al. Understanding the mechanism of retinal
691 displacement following rhegmatogenous retinal detachment repair: A computer simulation model.
692 Acta Ophthalmol 2021.
693 38. Rinkoff J, Machemer R, Hida T, Chandler D. Temperature-Dependent Light Damage to the
694 Retina. American Journal of Ophthalmology 1986;102(4):452-62.
695 39. Acharya S, Rayborn ME, Hollyfield JG. Characterization of SPACR, a sialoprotein associated
696 with cones and rods present in the interphotoreceptor matrix of the human retina: immunological and
697 lectin binding analysis. Glycobiology 1998;8(10):997-1006.
698 40. Hollyfield JG. Hyaluronan and the functional organization of the interphotoreceptor matrix.
699 Invest Ophthalmol Vis Sci 1999;40(12):2767-9.
700 41. Coles JM, Chang DP, Zauscher S. Molecular mechanisms of aqueous boundary lubrication
701 by mucinous glycoproteins. Current Opinion in Colloid & Interface Science 2010;15(6):406-16.
702 42. Wang ZY, Zhao PQ. Perfluorocarbon-air exchange in head side-turned position: a simple
703 technique to avoid retinal slippage. Retina 2010;30(1):177-9.

704

705

Figure Captions

Figure 1. *Ex vivo* model of retinal detachment. Experimental setup to assess retinal temperature, retinal thickness, and adhesion strength between retina and the RPE following RTF (dehydration then laser photocoagulation). A 6 x 12 mm section of retina with RPE, choroid and sclera in porcine and human cadaver eyes served as an ex vivo model of retinal detachment. The retinal sample was imaged using OCT (**A**), colour microscopy (**B**), and a thermal camera (**C**) simultaneously. The left edge of retina was RTF treated and pulled from the underlying RPE and choroid via an 8/0 suture attached to the retinal surface. **D.** The maximum force required to completely detach the retina was recorded using a force transducer, which allows quantification of the adhesion strength produced by RTF. RPE: retinal pigmented epithelium; RTF: retinal thermofusion; OCT: optical coherence tomography

Figure 2: Schematic of *in vivo* induction of rhegmatogenous retinal detachment and its repair with retinal thermofusion (RTF) in rabbits. After lensectomy (**A**) and vitrectomy (**B**), retinal detachment was induced by subretinal injection of normal saline (**C**) and retinotomy (**D**). Fluid-gas exchange was performed and excessive subretinal fluid was extruded prior to repair (**E**). The tear margin was further treated with 1940 nm laser photodehydration in continuous mode to eliminate the subretinal fluid meniscus (**F**), which facilitates an instant sealing after 1940 nm photocoagulation (**G**). A video of the surgery is available in Supplementary Video 3.

Figure 3. Effect of warm air dehydration on retinal thickness. A. Representative OCT images before and after 3 minutes of dehydration. Total retinal thickness at the edge treated by warm air flow was determined at 5 locations each 50 μm form the edge of the retinal margin. **B.** There was a gradual reduction of retinal thickness over the time course of dehydration (n = 15). OCT: optical coherence tomography; error bars: standard error of means; measurement lines are colour coded in panel B as per A.

Figure 4. Adhesion strength of retinal thermofusion in *ex vivo* porcine eyes. A. Following treatment cyanoacrylate glue was applied and a fiber connecting the retina to the force transducer was attached. A micromanipulator pulls at a constant rate causing the stress lines between the dried glue and the RTF treated retinal edge. **B.** Force traces for two samples, showing that the peak adhesion force was higher from RTF (grey trace) than laser coagulation alone (blue trace). **C.** Peak force measured for untreated (n = 9), photocoagulation alone (n = 5), warm air drying (1 minute n = 6, 2 minutes n = 9, 3 minutes n = 5) and RTF (n = 5). There was stronger adhesion with RTF compared with warm air drying and photocoagulation alone. **D.** The peak force achieved was associated with the temperature-time integral of drying prior to photocoagulation. RTF: retinal thermofusion; RPE: retinal pigmented epithelium; error bars: standard error of means; figure legend in panel D is as per panel C.

Figure 5. Comparison of retinal thermofusion achieved with warm air dehydration or laser photodehydration. A: Using our *ex vivo* porcine retina preparation we show that **s**imilar levels of adhesion force were achieved when dehydration for 3 minutes with warm air (n = 5), 1470 nm (n = 6) or 1940 nm lasers (n = 4). Higher force was achieved when dehydration was followed with photocoagulation (warm air dehydration followed by 810 nm photocoagulation [n = 5], 1470 nm [n = 13] and 1940 nm [n = 14] photodehydration followed by 532 nm photocoagulation). **B:** Retinal adhesion force achieved was similar between 810 (n = 8) and 532 nm (n = 11) photocoagulation laser. error bars: standard error of means.

Figure 6. Effectiveness of photodehydration followed by 532 nm or 1940 nm laser photocoagulation in *ex vivo* porcine and human retina. A. Donor tissue with model retinal tear to the left. Margin of dehydration and repair indicated by the blue arrow. The green arrows indicate margins of a new retinal tear induced by a tangential pull. The retina was bunched to the right of the cyanoacrylate glue. **B.** Haematoxylin and eosin staining of a retinal cross section showing bonding of the retina to the RPE and choroid. **C.** Photodehydration of porcine tissue produced higher adhesion force (untreated n = 9, 1940 nm dehydration n = 4, 1940 nm dehydration and 532 nm photocoagulation n = 14, 1940 nm dehydration and photocoagulation n = 12). **D.** Photodehydration followed by photocoagulation produced significantly higher adhesion (group sizes, untreated n = 4, 532 nm photocoagulation n = 4, 1940 nm dehydration and 532 nm photocoagulation n = 7, 1940 nm dehydration and photocoagulation n = 10).

Figure 7. *In vivo* retinal thermofusion in rabbit eyes. A. In two eyes *in vivo* RTF produced peak forces of 2.12 g (orange) and 4.39 g (yellow) adhesion force, compared with the control (0.79 g, grey trace). **B.** Summary of completed RTF surgeries in 17 animals. All surgeries using photodehydration (either 1470 nm or 1940 nm) followed by 532 nm coagulation or 1940 nm for both drying and coagulation. The primary outcome was confirmation that the entire retinal tear margin was attached as confirmed by in vivo fundoscopy as well as post-mortem histology. With the 1940 nm laser (followed by coagulation with either the 532 or the 1940 nm laser) all repairs were attached. Whereas when using 1470 nm for drying and 532nm for coagulation, two of the six repairs had detached retinas at the endpoint.

Figure 8. *In vivo* retinal thermofusion repair in the rabbit model. Two representative eyes are shown (A and B). i. *In vivo* fundus image of the retinal tear two weeks following RTF repair using 1940 nm photodehydration followed by 1940 nm photocoagulation. The pigmentary reaction around the edge of the retinal tear was evident. **ii.** Post-mortem eyes with the anterior segment removed showing intact retina and attached retina tear margin (arrow). **iii.** Eye cup with relaxing cuts prior to processing for histology, with the attached retinal tear (arrow). **iv.** Hematoxylin and Eosin-stained cross section (2x) through the retinal tear, with the edges of the tear indicated by the red and green arrows. Scale bar = 200 µM. **v-vii.** 10x magnification (v-vii) show repaired tear margin (red and green

777 arrows) and a region within the whole free of overlying retina. Black arrow region between repair
778 edges, red and green arrows RTF repair site edge. Scale bar = 50 µM.

779

Supplementary materials

Figure S1: Thermal impact of warm air and laser dehydration. **A.** Thermodynamic modelling demonstrating adiabatic expansion of highspeed air exiting a narrow tube (25G modelled). **B.** Thermal imaging (FLIR) of 60^{o}C air flow at 20 ml/min out of a 23G cannula onto a 6 x 12 mm (dotted region) post-mortem porcine retinal sample. With the probe held 1.5 mm from the surface of the retina tissue temperatures reached 35-45^{o}C over an area 4.5 - 5 mm. **C.** Thermal imaging of the 1940 nm laser at 5 mW, with the probe tip held at 1.5 mm from the tissue. The thermal footprint using laser dehydration was smaller (~1.5-2.0 mm).

Figure S2: Effect of laser dehydration with and without airflow. **A.** Laser wavelengths were chosen to target peaks in the absorption spectra of water. **B.** Images collected 1 minute following the onset of dehydration of a 20 μl water drops (left drops). The drop on the right provides a control. The inset shows thermal imaging (FLIR) of the same droplets. Room temperature (22^{o}C) airflow alone (10 ml/min), has little on the size of the drop. **C.** Drying using the 1470 nm laser at 45 mW reduced the size of the drop and produced condensate droplets around the periphery of the main drop. Peak temperature within the drop was 32^{o}C. D. The addition of 10ml/min air flow (22^{o}C) along with 1470 nm laser dehydration resulted in further reduction of drop size (32^{o}C) with fewer droplets in the surround. **E.** Laser dehydration with 20 ml/min airflow evaporated the drop and prevented any droplets formation within a minute.

Figure S3: Histology of *in vivo* retinal detachment repair. Animals were followed for 2 weeks following retinal detachment repair using retinal thermofusion (1940 nm laser photodehydration followed by laser photocoagulation. Each row shows Hematoxylin and Eosin-stained retinal cross sections taken through the site of retinal repair for one representative animal. The first column shows a lower magnification image through the retinal defect (black arrow) with the edges (red arrows) that were repaired. Scale bar = 200μM. The 2nd, 3rd and 4th columns show closeup images of the retinal defect, along with the two retinal tear margins. Scale bar = 50μM.

Figure S4: Retinal thermofusion increases adhesion through perfluorinated carbon liquid (PFCL. A. Fresh porcine retinal samples (6x12 mm) were placed with one edge upright in a well. Following treatment cyanoacrylate glue was applied and a fibre connecting the retina to the force transducer was attached. A micromanipulator pulls at a constant rate to measure force. The upper edge of the sample was (1) left untreated, (2) dried for 3 minutes using a 1940 nm laser in air or (3) dried for 3 minutes using a 1940 nm laser with the entire sample submerged under PFCL (Okta-line, Bausch and Lomb, Berlin, Germany). **B.** Compared with untreated samples, retinal thermofusion (RTF) increased force when applied either in air of through PFCL). One-way ANOVA p = 0.04.

Figure S5: Retina thickness as a function of distance from the edge of the RTF repair.

A. Images of H&E stained cross sections at 10x were assessed in control eyes (n=4) and in 5 eyes that had undergone retinal thermofusion (n=5) and left to stabilize for 14 days. Retinal thickness was measured every 0.5mm form the edge of the repair. **B.** Compared with normal retina, retinal thickness inside the lesion was significantly thinner (post-hoc, $p<0.05$). All other regions were not significantly thinner than normal control retinae. One way ANOVA ($p <0.001$), post-hoc control vs 0 mm $p<0.001$. all other regions vs control $p>0.05$.

Supplementary Video 1: *Ex vivo* porcine model of retinal detachment repair. The upper left panels show a single optical coherence tomography B-Scan measuring the edge of the retina and the underlying sclera (going from left to right of the sample). The lower left panel shows the tissue sample imaged from above using a thermal camera. The peak temperature is shown in the inset. The panel on the right shows the retina sample imaged through a surgical microscope to shows the change to eth retinal tissue surface induced by photodehydration and photocoagulation. The abbreviated sequence shows the drying phase followed by the photocoagulation phase of the RTF repair process.

Supplementary Video 2: higher adhesion is achieved with retinal thermofusion. *Ex vivo* porcine model of retinal detachment repair for showing change in force as the retina is pulled tangentially away for the site of repair at a rate of 0.1 mm/s, over the course of 60 seconds. The upper panels show force traces, and the lower panels show the retinal surface with 8/0 suture attached to the retinal surface using cyanoacrylate glue. The two panels on the left show a control untreated sample and those on the right a sample that had undergone retinal thermofusion (RTF, drying followed by photocoagulation). With progressively higher applied force the control sample slides, whereas the RTF retina break before the adhesion at the repair margin is broken.

Supplementary Video 3: In vivo rabbit model of retinal detachment repair. 25G cannulas were secured to the sclera. Phacoemulsification and lensectomy was performed through an incision just posterior to the limbus. Triamcinolone was used to facilitates removal of the clear vitreous. Saline was injected subretinal to create a bleb. A vitrector was used to create a retinotomy. The edge of the retinotomy was dried using retinal thermofusion; 1940 nm laser with 20 ml/min coaxial room temperature sterile airflow. The 1940 nm laser was then used to coagulate the retinal tear margin at a higher power setting. The eye was refilled using saline, cannulas removed and sclerotomies sutured. The retina can be seen to be attached 2 week following surgery.

Supplementary Video 4: In vivo rabbit model of retinal detachment repair. The edge of the retinotomy was dried using retinal thermofusion; 1940 nm laser with 20 ml/min coaxial room temperature sterile airflow. The 1940 nm laser was then used to coagulate the retinal tear margin at a higher power setting.

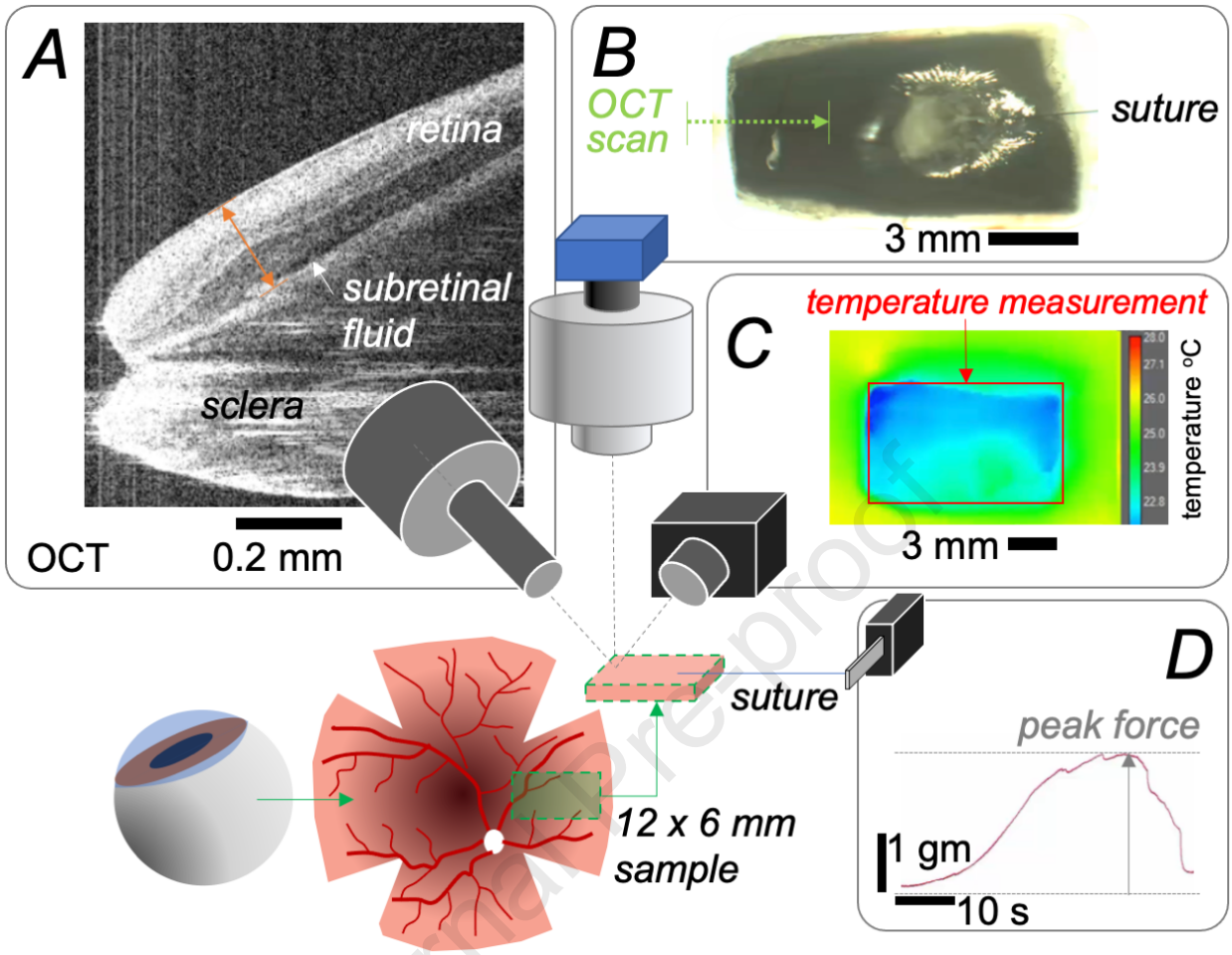

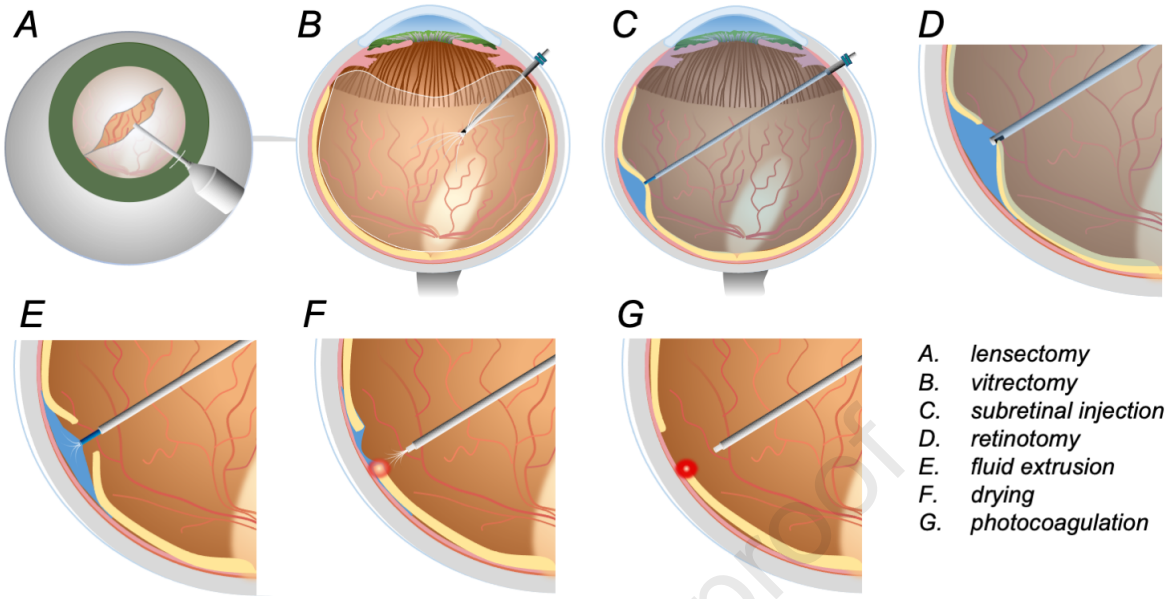

A. *lensectomy*
B. *vitrectomy*
C. *subretinal injection*
D. *retinotomy*
E. *fluid extrusion*
F. *drying*
G. *photocoagulation*

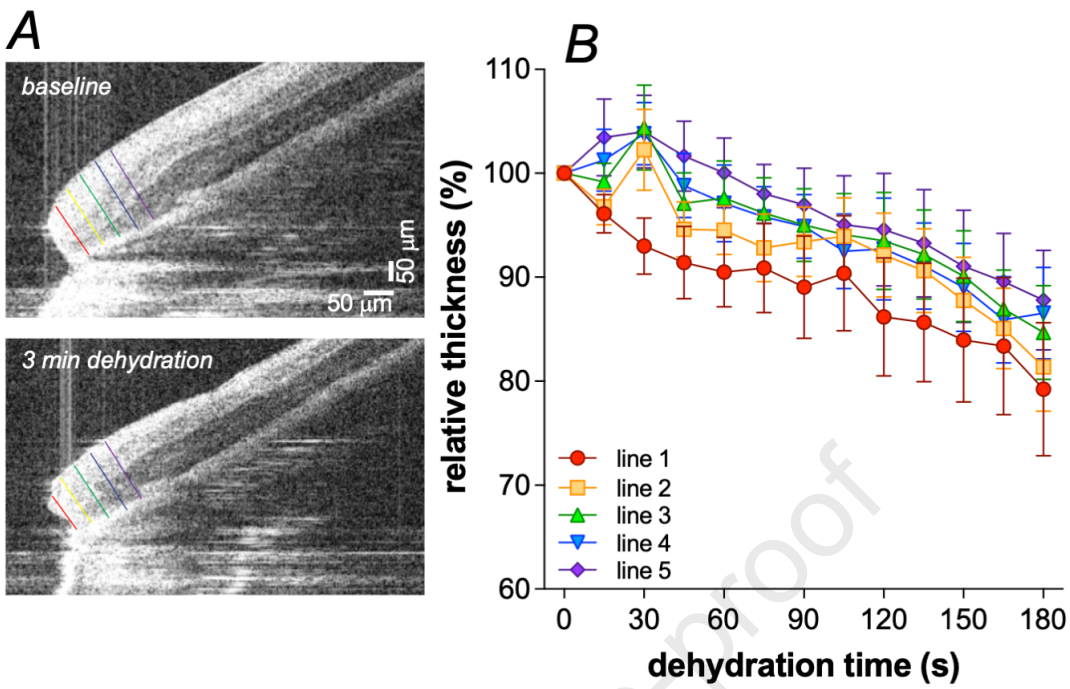

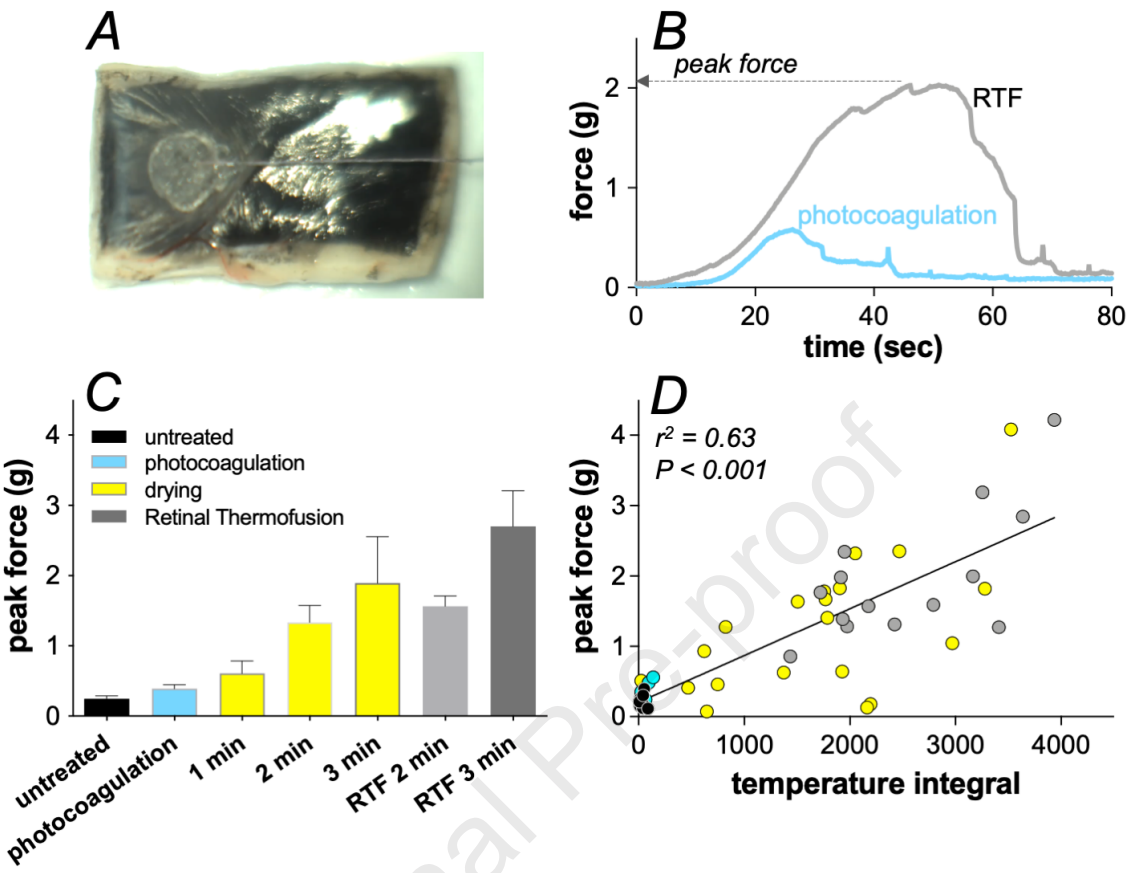

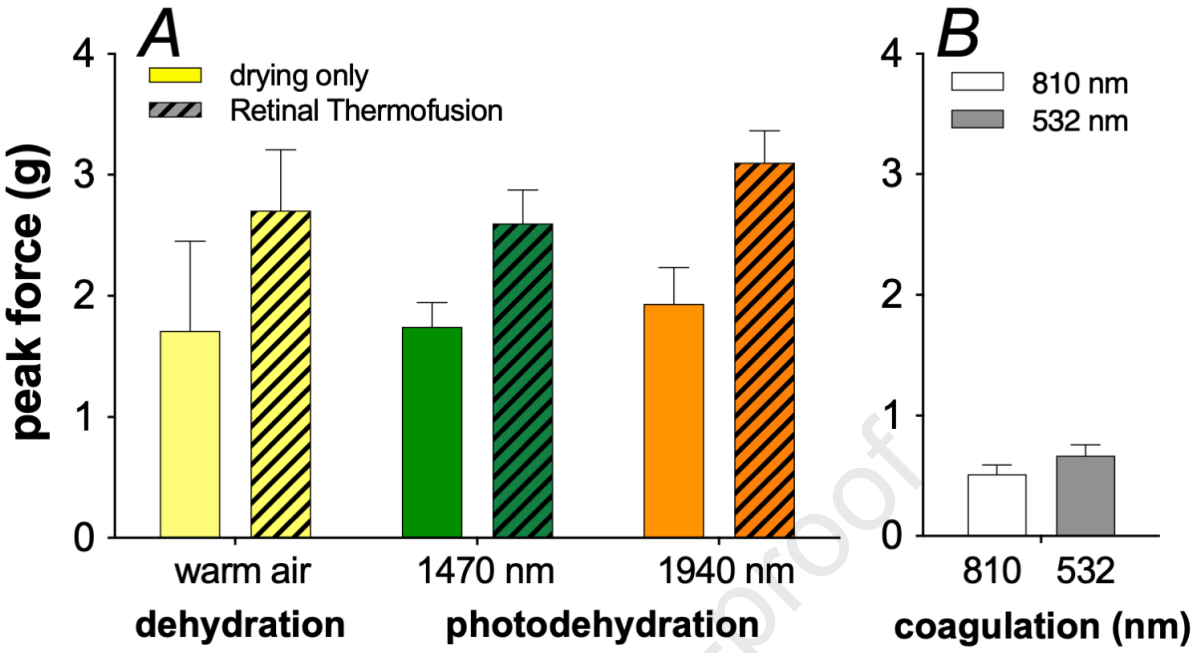

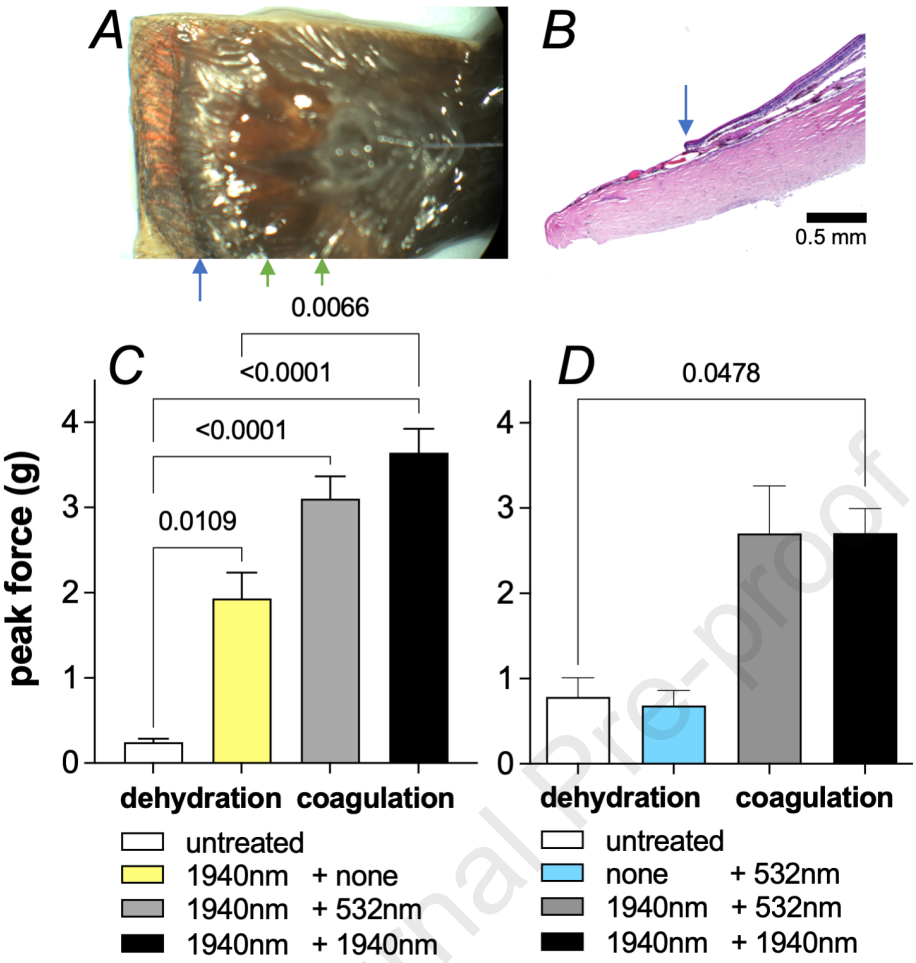

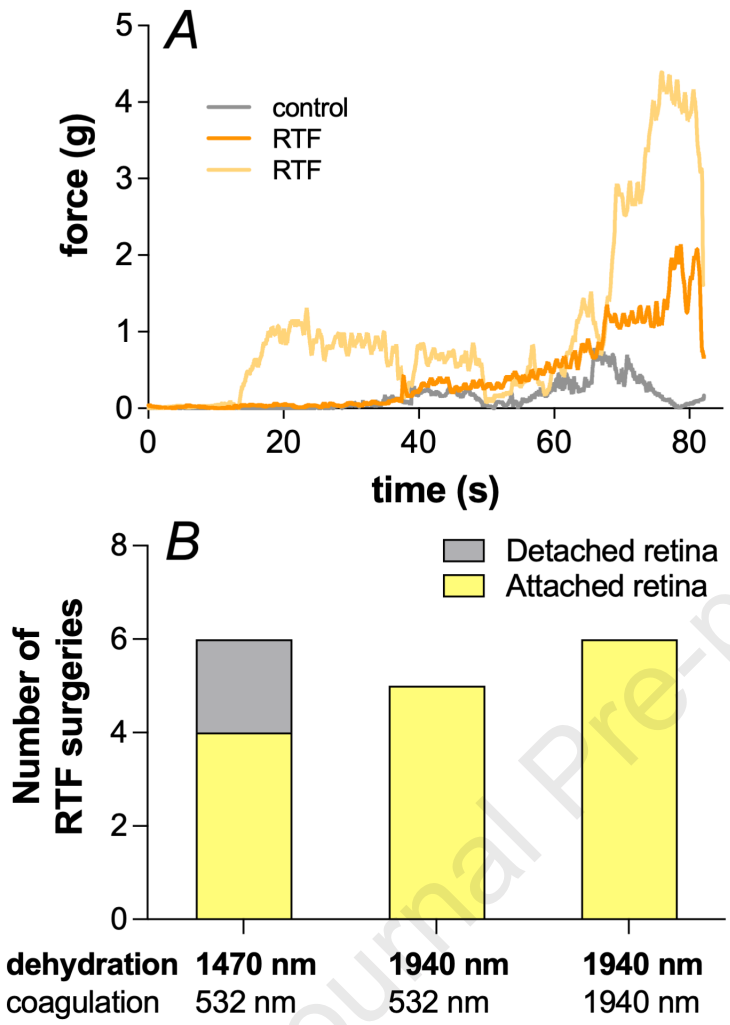

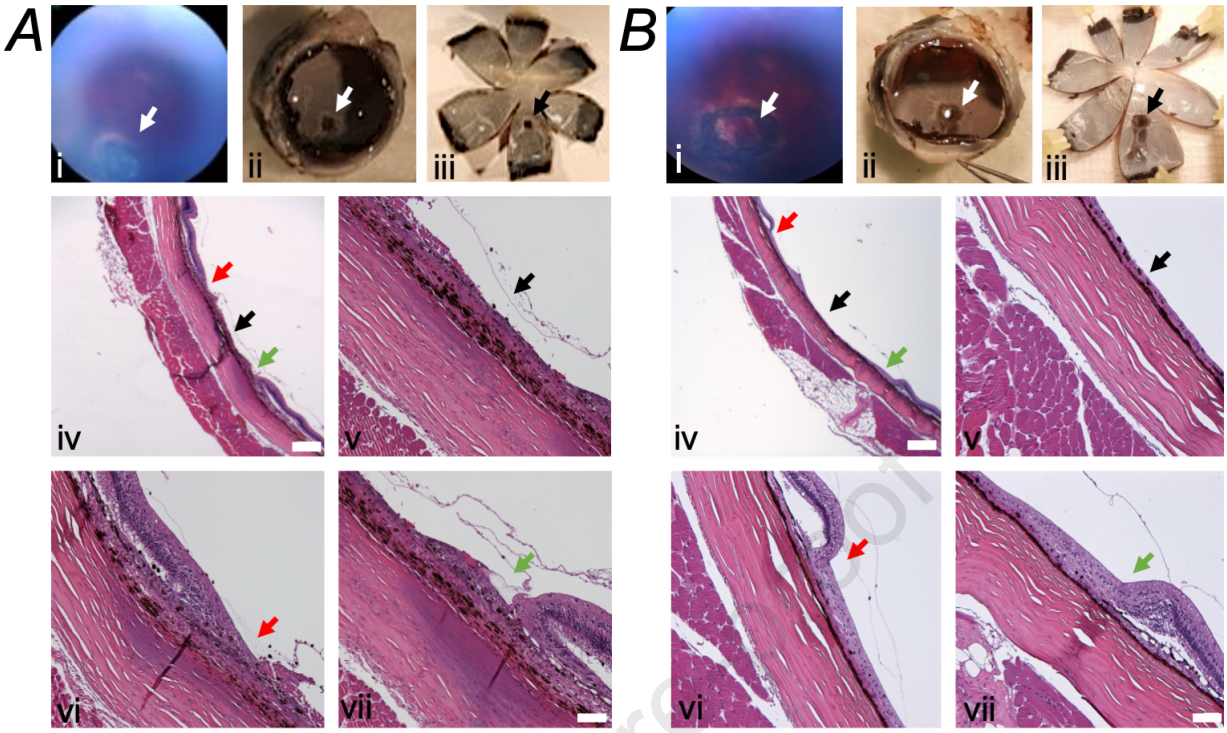

Retinal thermofusion laser dehydrating retinal tear margins prior to laser photocoagulation creates an immediate intraoperative waterproof retinopexy without tamponade. This approach has the potential to allow rapid postoperative recovery and return to a normal lifestyle.